

Design of prestressed gridshells as smooth poly-hypar surface structures

Journal Article**Author(s):**

Cao, Ting; D'Acunto, Pierluigi; Castellón, Juan J.; Tellini, Alessandro; Schwartz, Joseph; Zhang, Hong

Publication date:

2021-04

Permanent link:

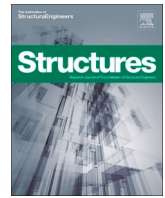
<https://doi.org/10.3929/ethz-b-000469370>

Rights / license:

[Creative Commons Attribution-NonCommercial-NoDerivatives 4.0 International](#)

Originally published in:

Structures 30, <https://doi.org/10.1016/j.istruc.2021.01.047>



Design of prestressed gridshells as smooth poly-hypar surface structures

Ting Cao^{a,*}, Pierluigi D'Acunto^a, Juan José Castellón^b, TelliniAlessandro Tellini^a, Joseph Schwartz^a, Hong Zhang^c

^a ETH Zurich, Stefano-Franscini-Platz 5, 8049 Zürich, Switzerland

^b Rice University, 6100 Main St, Houston, TX 77005, USA

^c Southeast University, Sipailou 2#, Xuanwu district, Nanjing, 211189, China

ARTICLE INFO

Keywords:

Smooth poly-hypar surface
Hyperbolic paraboloid
Prestressed gridshell
Surface structure
Lightweight structural design
Graphic statics
Design for reuse

ABSTRACT

This article demonstrates the design potentials of a recently developed approach for generating *smooth poly-hypar surfaces*, freeform surfaces made of combinations of hyperbolic paraboloids (hypars). In a smooth poly-hypar surface, the double curvature of the individual hypar modules and the smooth connections between them ensure global bending-free structural behaviour. In this article, the structural analysis of a prestressed gridshell as a smooth poly-hypar surface is introduced. Graphic statics is used to evaluate and control the distribution of internal forces within the structure. Moreover, a case study, the *Hypar Pavilion*, is presented as a prestressed gridshell as a smooth poly-hypar surface structure. The Hypar Pavilion was prefabricated using lightweight materials and low-tech manufacturing techniques. The entire gridshell was manually built out of forty individual hypars, which were combined following a specific sequence to ensure the kinematic stability of the ongoing construction without scaffolding.

1. Introduction

1.1. Design of double-curved surface structures

With the development of materials and construction techniques in the 20th century, surface structures such as shell and membrane structures have drawn increasing attention from engineers and architects [4]. The most well-known approach to deal with such systems are the *form-finding methods* introduced and developed by structural engineers and architects such as Frei Otto, Heinz Isler and Sergio Musmeci, among others [14]. As these form-finding methods are generally carried out considering given dominant load cases, the resulting forms are only bending-free for specific load configurations. Moreover, due to their double-curved freeform geometries, they generally require complex formwork and scaffolding to be constructed.

As an alternative to form-finding, a few structural engineers and architects of the 20th century explored the spatial and structural potentials of *hyperbolic paraboloids (hypars)* for the design of double-curved shells. Contrary to form-finding, in this approach, the structures are not the result of a self-forming process but they are defined based on the geometric properties of the hypars [23]. This approach leads to the

generation of structures that are able to support variable loadings with only membrane forces [2,10,9,34,39,40]. Furthermore, being double-curved and double ruled surfaces, hypars can be fabricated in a relatively simple way, while at the same time ensuring structural integrity. As shown by the remarkable work of Felix Candela [29], Eduardo Torroja [1], Pier Luigi Nervi [6], among others, hypars can be effectively used for the design of complex shell structures.

1.2. Combinations of hypars as surface structures

An approach to the design of freeform surfaces as combinations of hypars – *smooth poly-hypar surfaces*, also referred to as *hyperbolic nets* [25] or *A-nets* [24], – has been recently introduced from a structural perspective [12,13,11]. While in the existing precedents, hypars are generally joined through folds that work as stiffening beams, leading to bending actions at the edges [3,7,35,31,36,38,37,19], in the smooth poly-hypar surfaces, different hypars are combined smoothly. This approach results in freeform surfaces through a geometrically controlled composition of hypars while guaranteeing overall bending-free behaviour of the structure. Similar geometrical approaches can be found in the past in some of the sculptures designed and built by the artist Angel

* Corresponding author.

E-mail addresses: caoting@arch.ethz.ch (T. Cao), dacunto@arch.ethz.ch (P. D'Acunto), jcastellon@rice.edu (J.J. Castellón), tellini@arch.ethz.ch (T. Tellini), schwartz@arch.ethz.ch (J. Schwartz), zhangh555@seu.edu.cn (H. Zhang).

<https://doi.org/10.1016/j.istruc.2021.01.047>

Received 29 May 2020; Received in revised form 23 December 2020; Accepted 13 January 2021

Available online 9 February 2021

2352-0124/© 2021 The Authors. Published by Elsevier Ltd on behalf of Institution of Structural Engineers. This is an open access article under the CC BY-NC-ND

license (<http://creativecommons.org/licenses/by-nc-nd/4.0/>).

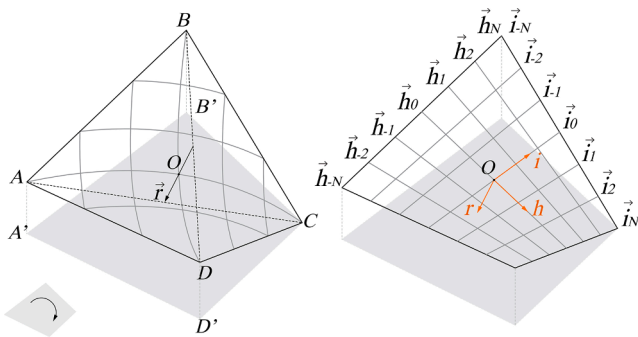


Fig. 1. A hyperboloid contains two sets of rulings and two sets of parabolas (left). To describe the geometry and internal forces of a hyperboloid, a coordinate system with origin O and three coordinate axes i, h, r is set up. All the rulings can be represented as vectors towards the positive direction of h and i (right).

Duarte [20]. Moreover, related geometrical research has been carried out on the approximation of freeform surfaces with hyperboloids [41,22,26,24].

Structurally, a cluster of hyperboloids as a smooth poly-hyperboloid surface behaves similarly to its basic hyperboloid module. It is a form-active system that can be implemented as either continuous shells or gridshells [5]. This article focuses on prestressed gridshells designed with smooth poly-hyperboloid surfaces, explaining their structural behaviour and showing their architectural application in a case study, the *Hypar Pavilion*.

1.3. Graphic statics

The structural analysis developed in this article is entirely based on *graphic statics* and relies on the *theory of plasticity* [32]. *Graphic statics* is a synthetic vector based structural analysis and design method, which can be described as a set of geometric procedures based on vectors and projective geometry [28,16,15]. It provides intuitive visual information about the relation between form and forces, which makes the interaction between architectural and structural thinking explicit starting from the early phase of the design process [21].

Various approaches have been defined to extend graphic statics to the third dimension [27]. In this article, the vector-based approach to 3D graphic statics [18] is used to control the internal forces within the proposed smooth surfaces made of combination of hyperboloids.

1.4. Content

The remainder of the article is organised as follows. In Section 2, the geometrical definitions and structural behaviour of hyperboloids are presented. The concept of smooth poly-hyperboloid surfaces is then introduced together with two constraints, which enable an abstract smooth poly-hyperboloid surface becoming an efficient structure with only membrane forces. Grounded on these geometrical and structural concepts, Section 3 explains in detail the structural analysis of a prestressed smooth poly-hyperboloid gridshell using graphic statics. Section 4 presents the global design of the *Hypar Pavilion*, a prototype based on smooth poly-hyperboloid surfaces. This section includes the conceptual design, the structural modelling, and construction of the pavilion. Eventually, in the last section conclusions are drawn on the main structural advantages to design prestressed gridshells as smooth poly-hyperboloid surfaces, comparing similarities and differences between the prestressed gridshells and continuous shells in terms of their structural behaviour.

2. Smooth poly-hyperboloid surface structures

2.1. Hyperboloid of one sheet (hypar)

A hyperboloid is a double curved and double ruled surface, which can be

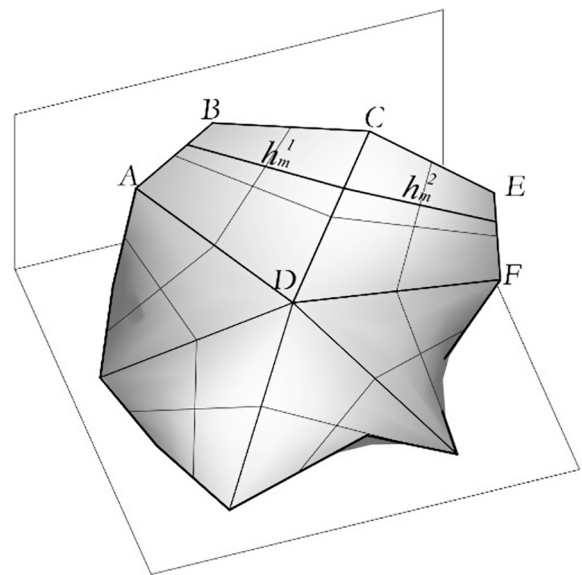


Fig. 2. A smooth poly-hyperboloid surface. Based on the coplanarity principle, any ruling h_m^1 of a hyperboloid $ABCD$ and ruling h_m^2 of a hyperboloid $CDEF$ are always coplanar with their shared edge DC . This property ensures that adjacent hyperboloids are connected smoothly.

constructed geometrically after defining four non-coplanar points ($A, B, C,$ and D), in such a way that the projections of these four points on the horizontal plane are arranged in a clockwise orientation (Fig. 1 right). Every two consecutive points are connected by an edge of a hyperboloid. After connecting the two pairs of points, which are not extremes of the same edge, the two diagonals AC and BD of the hyperboloid are obtained. The vector from the middle point of diagonal BD to the middle point of AC is the axis \vec{r} of the hyperboloid, which passes through the centre O (Fig. 1 right). Axis \vec{r} is a fundamental geometrical parameter of the hyperboloid and it is directly related to its structural behaviour [10]. When planes parallel with plane AOr and plane BOr intersect a hyperboloid, the intersecting curves define two sets of parabolas. The axes of all the parabolas of a hyperboloid are always parallel to axis \vec{r} (Fig. 1 right).

Similarly, one set of straight rulings h_m can be obtained by intersecting a hyperboloid with planes parallel to the plane Ohr , and another set of rulings i_n are the intersecting lines of the hyperboloid and planes parallel to the plane Oir , ($m, n \in \mathbb{Z}$), (Fig. 1 left).

In the structural analysis of a hyperboloid with graphic static, a coordinate system with origin O and three coordinate axes r, h and i is set up to describe the geometry and the internal forces of the hyperboloid (Fig. 1 left), with the conditions that $\vec{h} \cdot \vec{BC} > 0$ and $\vec{i} \cdot \vec{AB} > 0$.

As proved by Felix Candela [9], the loads applied on a continuous hyperboloid shell are carried not only by two sets of parabolas, but also by two groups of rulings. In this way, an individual hyperboloid in any arbitrary position in space behaves structurally between a wall and a shell, with the reactions only parallel to the rulings and edges [9,12].

2.2. Combination of hyperboloids as smooth poly-hyperboloid surfaces

Based on the structural behaviour of an individual hyperboloid, a new category of freeform surfaces, smooth poly-hyperboloid surfaces, is developed to design efficient smooth surface structures. This approach utilises hyperboloids as basic modules to generate smooth double-curved surfaces. Such smoothness satisfies the second order of continuity - i.e. G^2 continuity and tangency [30]. A smooth poly-hyperboloid surface is globally freeform, but it is also locally ruled, by benefiting from the nature of the individual hyperboloids as ruled surfaces (Fig. 2). As such, a smooth poly-hyperboloid surface allows only membrane forces to be transferred within the surface. Such property relies on the structural behaviour of an

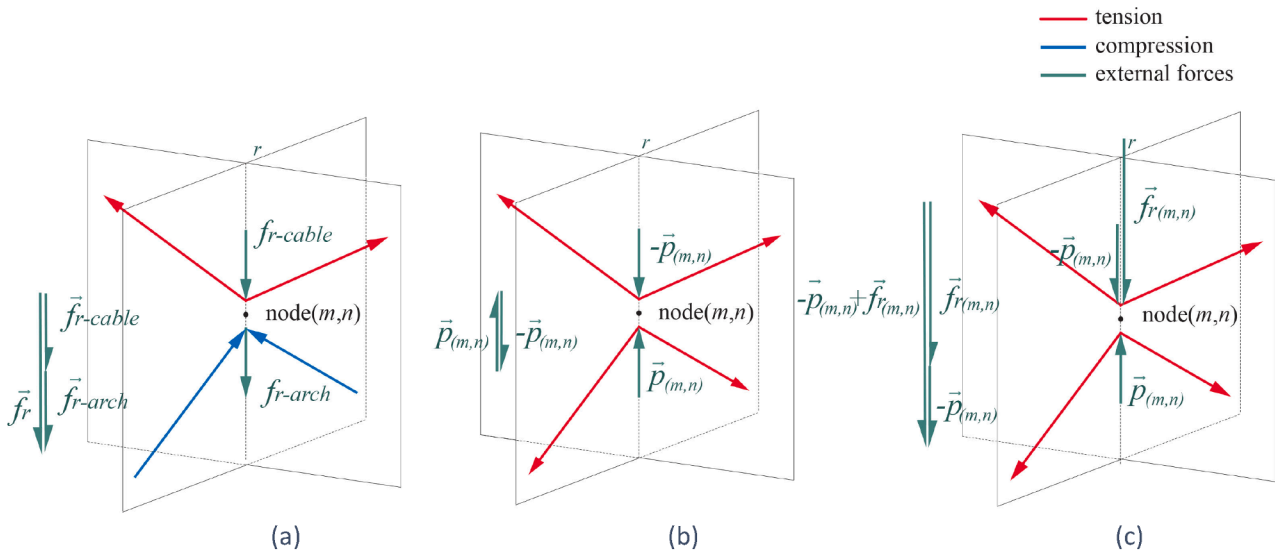


Fig. 3. Loads distribution at one node of a hypar. Considering one node in a continuous shell, the parabolic compressive arch and the tensile cable each takes half of the load parallel to axis \vec{r} (left). Considering one node in a self-stressed hypar without additional loads, the two parabolas are prestressed and both in tension, with the sum of two prestressing forces \vec{p} and $-\vec{p}$ being equal to zero (middle). Considering one node in a prestressed hypar with self-weight, the cable curving downward is prestressed with \vec{p} , while the cable curving upward is prestressed and loaded with a component parallel to axis \vec{r} (right).

individual hypar as well as the global stability of the smooth poly-hypar surfaces. To ensure bending-free behaviour of the generated poly-hypar surfaces, two constraints must be fulfilled: the *coplanarity principle* and fully supported *load paths* [13].

The coplanarity principle ensures that the connection between each pair of adjacent hypars is always smooth. It requires rulings and edges in a smooth poly-hypar surface intersecting at one node always be coplanar (Fig. 2). In order for two adjacent hypars to satisfy the coplanarity principle, the edges of the hypars, represented as vectors, should satisfy the following linear combination (Fig. 2), with k, j, l scalars and k less than zero [13]:

$$\vec{CE} = k\vec{CB} + j\vec{CD} \quad \vec{DF} = k\vec{DA} + l\vec{DC}$$

The load path is in relation to the global equilibrium of a smooth poly-hypar surface. Considering each hypar as a sub-system in equilibrium, the reactions at the border of one hypar are transferred as actions into the adjacent hypars. In this case, hypars in a smooth poly-hypar surface are supported one by another until the internal forces are transmitted to the supports [13], (Fig. 6). Since the internal local forces along parabolas do not affect the global equilibrium, only interactions along rulings and edges are considered in the global equilibrium of smooth poly-hypar surfaces. Based on the coplanarity principle, all intersecting rulings and edges of two adjacent hypars are always coplanar. This geometric property implies that the interaction forces between adjacent hypars are always transmitted along rulings and edges, thus generating specific load paths to transfer the internal forces to the supports [13]. In this way, the designer can combine hypars freely

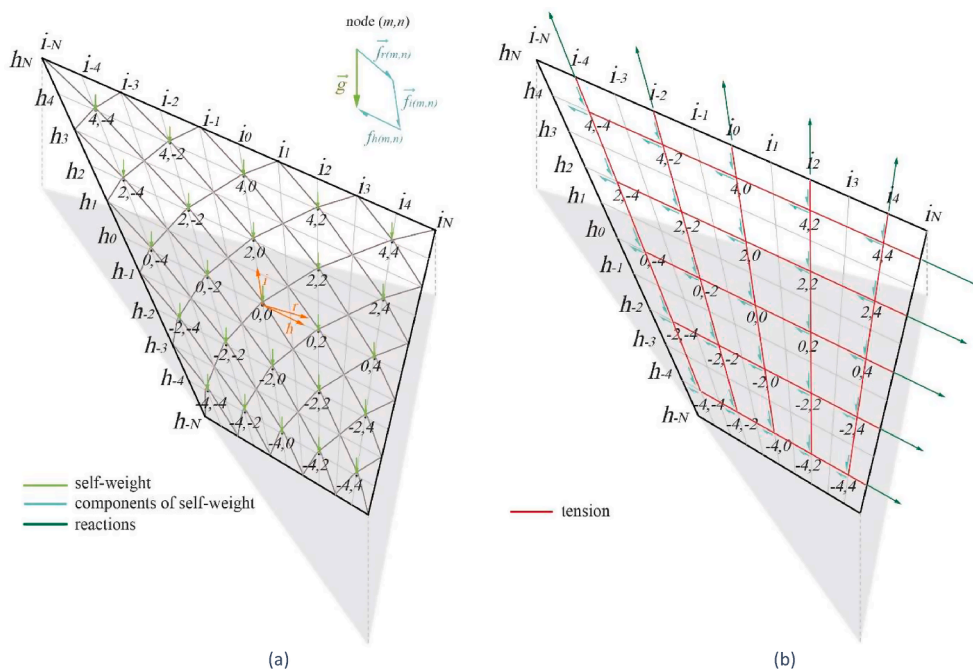


Fig. 4. Considering a coordinate system with three coordinates (h, i, r) , rulings \vec{h}_m and \vec{i}_n are represented as ruling vectors \vec{h}_m, \vec{i}_n (directed towards the positive directions of coordinate axes). Moreover, nodes where parabolas and rulings intersect, are numbered by a pair of coordinates (h, i) . The point load \vec{g} applied at any node (m, n) can be decomposed into ruling components $\vec{f}_{h(m,n)}, \vec{f}_{i(m,n)}$ and axis component $\vec{f}_{r(m,n)}$ (left). Subsystem I is only loaded with ruling components, which are balanced with reactions parallel to edges (right).

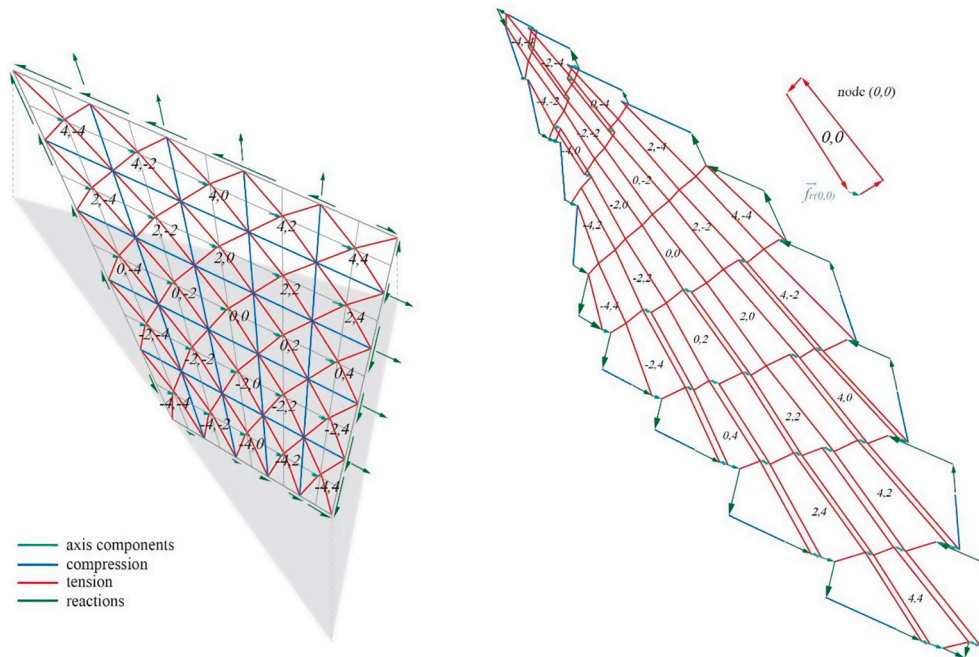


Fig. 5. Internal forces and reactions of Subsystem II. Vector-based 3D form diagram (left) and force diagram (right).

as long as the coplanarity principle is fulfilled and each load path is directly connected to a support.

3. Structural analysis of prestressed grid shells

Based on the geometrical and structural properties described above, the internal forces within a smooth poly-hypar surface can be analysed and controlled using graphic statics. In this section, a smooth poly-hypar surface is implemented as a prestressed gridshell. At first, one typical hypar module is analysed to describe the structural behaviour as a subsystem in equilibrium. The evaluation of the internal forces in the entire prestressed gridshell is then performed.

3.1. Single hypar as a prestressed gridshell module

Each of the hypars constituting a prestressed gridshell can be regarded as a prestressed module with rulings as struts and parabolas as cables. Unlike the case of a continuous shell with parabolic tensile cables and compressive arches (Fig. 3right), in the gridshell, all the parabolas work as prestressed cables (Fig. 3middle, left). If a self-stressed hypar is loaded with self-weight (Fig. 3left), prestressing forces vary among the different cables, depending on the self-weight and the geometry of the hypar.

To study the relation between the geometry of a hypar and its internal forces, a coordinate system (Section 2.1) is introduced to represent all rulings h_m, i_n as vectors \vec{h}_m, \vec{i}_n ($m, n \in \mathbb{Z}, N \in \mathbb{Z}$), and to number the nodes with coordinates h and i (Fig. 4). If there are $2N$ rulings in a hypar, the total weight of hypar is split into N^2 patches. To simplify the calculations, the weight of each patch is considered as the same, then combined as a point load \vec{g} applied at the centre of each patch (Fig. 4left). A point load applied at any node (m,n) can be divided into three components (Fig. 4left): ruling components $\vec{f}_{h(m,n)}$ and $\vec{f}_{i(m,n)}$ parallel to ruling vectors \vec{h}_m and \vec{i}_n respectively, and axis components $\vec{f}_{r(m,n)}$ parallel to axis \vec{r} of the hypar. According to the force decomposition illustrated in Fig. 4left, the three load components at this node can be expressed in relation to the scalars a, b, c of vectors \vec{h}_m, \vec{i}_n and \vec{r} as follows[11]:

$$\begin{aligned} \vec{f}_{h(m,n)} &= a \vec{h}_m & \vec{f}_{i(m,n)} &= b \vec{i}_n \\ \vec{f}_{r(m,n)} &= \left(c - \frac{am + bn}{N}\right) \vec{r} \end{aligned} \tag{4-1}$$

After applying ruling components $\vec{f}_{h(m,n)}, \vec{f}_{i(m,n)}$ and axis component $\vec{f}_{r(m,n)}$ separately onto the hypar, the entire hypar can be regarded as the superposition of two sub-systems in equilibrium: Subsystem I (Fig. 4right) loaded with the ruling components $\vec{f}_{h(m,n)}$ and $\vec{f}_{i(m,n)}$; Subsystem II (Fig. 5left) loaded with axis components $\vec{f}_{r(m,n)}$.

To achieve the equilibrium of Subsystem I, the reactions should have

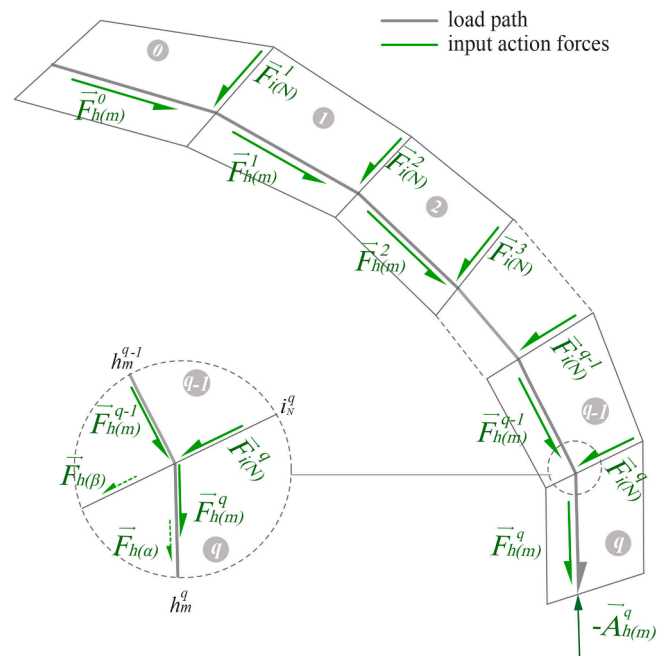


Fig. 6. A general case with q pieces of hypars along the same load path.

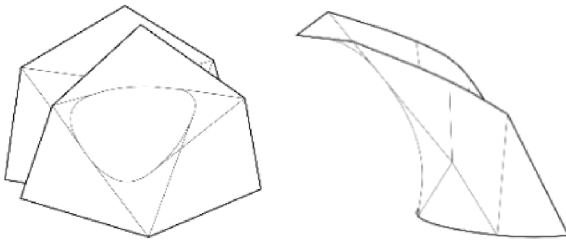


Fig. 7. Two different types of sub-prototypes within the Hypar Pavilion: hyperbolic void (left) and cantilever (right).

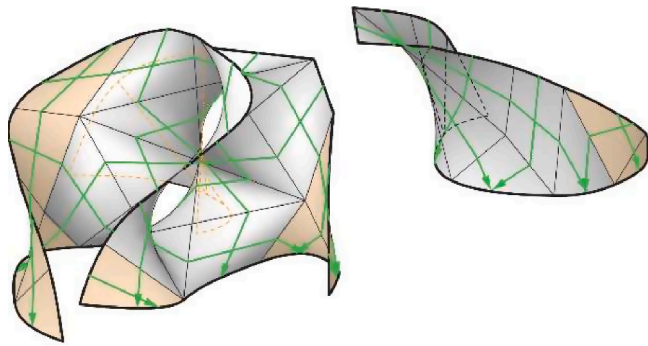


Fig. 8. The main vault was created by combing sub-prototypes: two hyperbolic voids and one cantilever. By adding extra 12 hypar modules (orange elements), all the load paths could be directly connected to the ground.

the same magnitude as the ruling components but reversed direction (Fig. 5right). Considering that there is N number of nodes along the same ruling, according to Eq. (4-1), the sum of all reactions along any ruling h_m and i_n , can be expressed as follows:

$$\vec{R}_{h(m),I} = -Na\vec{h}_m \quad \vec{R}_{i(n),I} = -Nb\vec{i}_n \quad (4-2)$$

Subsystem II is loaded with axis components and prestressing forces parallel to axis \vec{r} (Fig. 5left). To ensure only membrane forces in every parabola cable, prestressing forces $\vec{p}_{(m,n)}$ applied on cables curving downward should be the same at every node (m,n) of the same cable. Similarly, for cables curving upward, the sum of prestressing force $-\vec{p}_{(m,n)}$ and axis component $\vec{f}_{r(m,n)}$ should also be the same at every node (m,n) of the same cable (Fig. 5).

To achieve the configuration described above, by comparing the value of $\vec{f}_{r(m,n)}$ in Eq. (4-1), the prestressing force $\vec{p}_{(m,n)}$ applied at node (m,n) of a cable curving downward can be expressed as a function of $m-n$ as in (4-3). The difference of two coordinates $m-n$ is the same for every node on the same cable curving downward (Fig. 5). This ensures that $\vec{p}_{(m,n)}$ remains the same when coordinates m, n vary:

$$\vec{p}_{(m,n)} = [wc + (m-n)\frac{b-a}{2N}]\vec{r} \quad (4-3)$$

where w is a parameter introduced to control the amount of prestressing forces. According to Eq. (4-1) and Eq. (4-3), loads applied at the node (m,n) of the cables curving upward, which is the sum of prestressing forces $-\vec{p}_{(m,n)}$ and the axis components $\vec{f}_{r(m,n)}$, can be written as a function of $n+m$. ($n+m$ is the same for every node on the same cable curving upward, Fig. 5).

$$\vec{f}_{r(m,n)} - \vec{p}_{(m,n)} = [(1-w)c - (n+m)\frac{a+b}{2N}]\vec{r} \quad (4-4)$$

By varying the parameter w , Eqs. (4-3) and (4-4) can have multiple solutions, which implies that the designer can freely define the prestressing forces. Moreover, Eqs. (4-3) and (4-4) ensure that in

Subsystem II all cables are loaded with distributed loads parallel to axis \vec{r} .

After setting the value of w , and consequently, the prestressing forces in (4-3) for the cables curving downward, and (4-4) for the cables curving upward, it is possible to construct the vector-based 3D force diagram [18] shown in Fig. 5right, which suggests a linear description for the reactions in Subsystem II. The sum of reactions along any rulings h_m and i_n ($m, n \in Z$), (Fig. 5left) in Subsystem II are:

$$\vec{R}_{h(m),II} = -\frac{aN}{2}\vec{h}_m \quad \vec{R}_{i(n),II} = -\frac{bN}{2}\vec{i}_n \quad (4-5)$$

The sum of all reactions along edges h_N, h_N, i_N, i_N can be written as functions of the ruling vectors:

$$\begin{aligned} \vec{R}_{h(-N)} &= \frac{(2c+a)N}{4}\vec{h}_{-N} & \vec{R}_{i(-N)} &= \frac{(2c+b)N}{4}\vec{i}_{-N} \\ \vec{R}_{h(N)} &= \frac{(a-2c)N}{4}\vec{h}_N & \vec{R}_{i(N)} &= \frac{(b-2c)N}{4}\vec{i}_N \end{aligned} \quad (4-6)$$

After overlaying Subsystem I and II, it is possible to conclude that in a hypar regarded as a prestressed gridshell module, to achieve equilibrium under distributed loads, reactions are always parallel to the rulings and to the edges. The reactions along rulings are always a linear combination of ruling vectors, as shown in the Eq. (4-2), Eq. (4-5). The reactions along the edges are also a linear function of the vectors representing the geometries of the edges, as shown in the Eq. (4-6). In fact, the reactions are independent of the prestressing forces \vec{p} and $-\vec{p}$.

3.2. Global equilibrium of a smooth poly-hypar gridshell

In a smooth poly-hypar gridshell, considering each hypar module as a subsystem in equilibrium, the reactions at the border of one hypar are transferred as actions into the adjacent hypars. For example, for the hypar analysed in Section 3.1, reactions \vec{R}_h and \vec{R}_i along any rulings and edges can be reversed as input action forces \vec{F}_h and \vec{F}_i in the global equilibrium of the smooth poly-hypar gridshell [13,17]. Action forces \vec{F}_h and \vec{F}_i along rulings and edges of one hypar should be the same magnitude but opposite to the directions of reactions \vec{R}_h, \vec{R}_i .

In the global equilibrium of a smooth poly-hypar surface, forces along rulings are always transmitted along load paths (Section 2.2). A group of hypars along one load path is illustrated in Fig. 6 to show how to calculate internal forces in a smooth poly-hypar surface. In particular, the internal forces along rulings h_m ($m \in Z$) of this group of hypars is evaluated. Hypars along the same load path are numbered from the starting point of the load path to the support. Through the load path, in compliance with the coplanarity principle (Section 2.2), the action force $\vec{F}_{h(m)}^{(q-1)}$ along ruling h_m of hypar H_{q-1} can be decomposed into two components (Fig. 6):

$$\vec{F}_{h(m)}^{(q-1)} = \vec{F}_{h(\alpha)} + \vec{F}_{h(\beta)} \quad (4-7)$$

$\vec{F}_{h(\alpha)}$ is along ruling h_m of hypar H_q and $\vec{F}_{h(\beta)}$ is along edge i_N of hypar H_q . In this case, (4-7) can be rewritten as a function of input action forces $\vec{F}_{h(m)}^q$ and $\vec{F}_{i(N)}^q$:

$$\vec{F}_{h(m)}^{(q-1)} = s_q \vec{F}_{h(m)}^q + t_q \vec{F}_{i(N)}^q \quad (4-8)$$

where s_q and t_q are vector scalars; in the index of the action force $\vec{F}_{h(m),m}^q$, m represents the number of rulings; q represents the position of the hypar along the load path.

All the hypars that precede hypar H_q along the load path generate components that are eventually accumulated at the ruling h_m of hypar H_{q-1} . According to (4-7), internal forces accumulated along ruling h_k of hypar H_{q-1} can be written as the sum of $q-1$ parts components in (4-9):

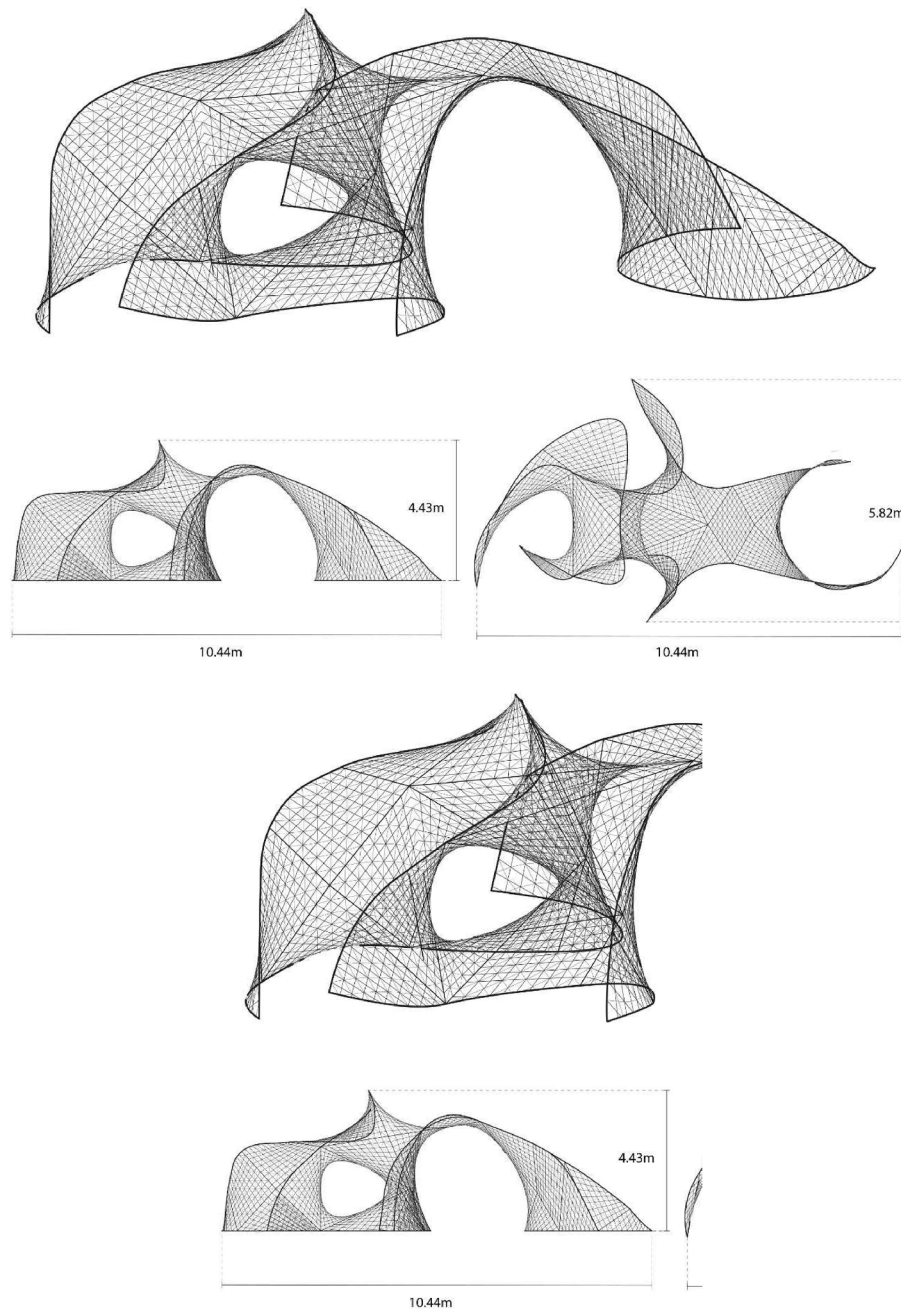


Fig. 9. The Hypar Pavilion as a gridshell, axonometric view (top), elevation (bottom left), plan (bottom right).

$$\vec{A}_{h(m)}^q = \left(1 + \sum_{j=1}^q \prod_{l=j}^q s_l \right) \vec{F}_{h(m)}^q \quad (4-9)$$

According to (4-9), internal forces accumulated along rulings h_m of hypar H_{q-1} can be expressed as:

$$\vec{A}_{h(m)}^{q-1} = \left(1 + \sum_{j=1}^{q-1} \prod_{l=j}^{q-1} s_l \right) \vec{F}_{h(m)}^{q-1} \quad (4-10)$$

In general, accumulated force $\vec{A}_{h(m)}^{q-1}$ along ruling h_m of hypar H_{q-1} can also be decomposed into two components along ruling h_m and edge i_N of hypar H_q (Fig. 6). Substituting $\vec{A}_{h(k)}^{q-1}$ in Eq. (4-10) for $\vec{F}_{h(m)}^{q-1}$ in (4-7), the deviation force along edge i_N of hypar H_q are obtained:

$$\vec{D}_{i(N)}^q = t_q \left(1 + \sum_{j=1}^{q-1} \prod_{l=j}^{q-1} s_l \right) \vec{F}_{i(N)}^q \quad (4-11)$$

The deviation force $D_{i(N)}^q$ along shared edge i_N of hypar H_q in Fig. 6 can be added with the action force $\vec{F}_{i(N)}^q$, and treated again as an input

Table 1
Dimensions and mass of the main construction materials.

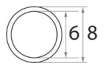

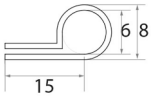
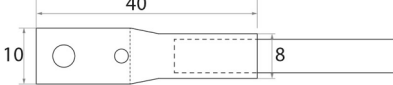

	Total length [m]	Total mass [kg]	Section [mm]
Aluminium rod	1003.17	60.67	
Steel cable	709.2	17.49	
Sum		78.16	

Table 2
Dimensions and masses of the connections.

	Amount	Total Mass [kg]	Dimension [mm]
R-shape connections	1460	0.98	
Rotating heads	810	4.39	
Cable rings	1820	0.05	
Sum		5.42	

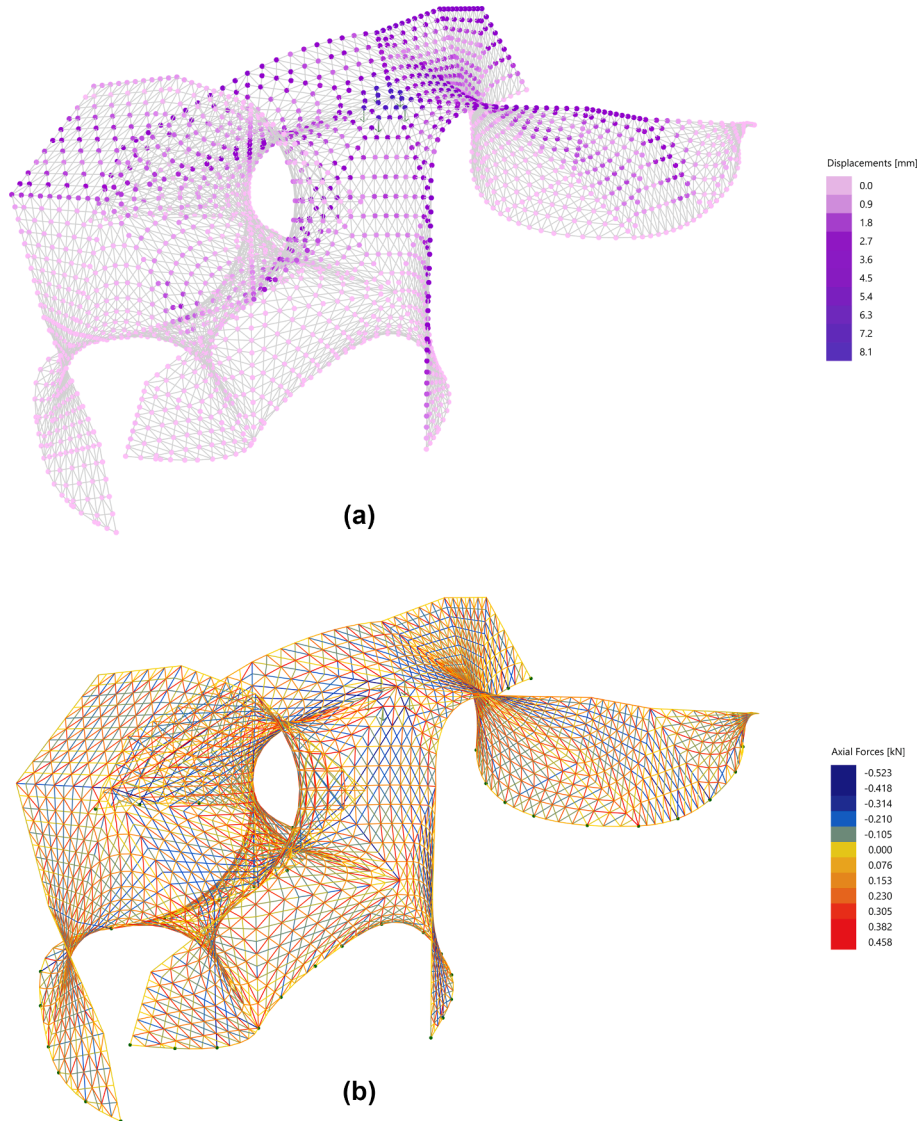


Fig. 10. Results of the Finite Element Analysis of the Hypar Pavilion, considering the self-weight, the prestressing of the steel cables, and a live load of five point loads simulating a mass hanging from the structure: displacements [mm] (up); internal axial forces [kN] (below).

action force along rulings and transmitted into the supports through other load paths. Using Eqs. (4-9) and Eq. (4-11) repeatedly, the final accumulated internal forces along rulings and edges can be calculated until the deviation forces along the edges are all connected with the supports directly.

4. Case study: the hypar Pavilion

4.1. Conceptual design

In order to test the applicability of smooth poly-hypar surfaces in real design scenarios, a lightweight aluminium gridshell, the Hypar Pavilion, has been built in Nanjing (China) as a temporary installation during a

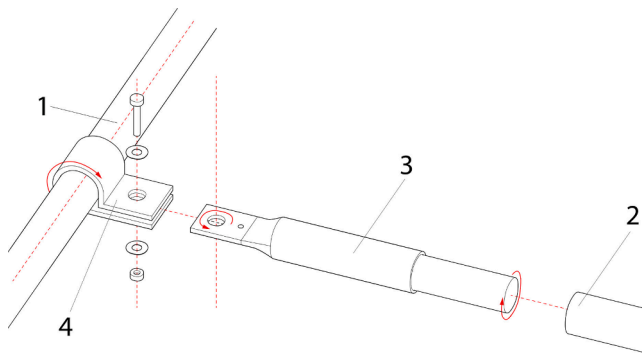


Fig. 11. The connection between an edge rod [1] and a ruling rod [2] included two hinges and one telescopic connection: one hinge in the R-shape connection [4], rotating around the axis of an edge rod; the other hinge in the rotating head [3], rotating around the axis of the rivet, and the other telescopic connection [2] rotating around the axis of a ruling rod.

two-week workshop organised by the Southeast University and ETH Zurich in June 2018.

The smooth poly-hypar surface of the pavilion is the composition of two sub-prototypes: a hyperbolic void and a cantilever (Fig. 7). After combining two hyperbolic voids and the cantilever, an additional vaulted surface is produced. To ensure that all the load paths reach the supports on the ground, twelve hypar modules were added to the structure (Fig. 8). On the one hand, these extra elements ensure that only membrane forces are transferred within the shell. On the other hand, these hypar modules produce more spatial differentiation and add to the

pavilion more potentials of use. The final pavilion was eventually composed of 40 hypar modules, and it had overall dimensions of 10.44 m by 5.82 m in plan and a maximum height of 4.43 m (Fig. 9).

The design of the Hypar Pavilion was developed within the commercial CAD platform *McNeel Rhinoceros* (<https://www.rhino3d.com/>, accessed 03.2020) and *McNeel Grasshopper* (<https://www.grasshopper3d.com/>, accessed 03.2020), using customised scripts based on *IronPython* (<https://ironpython.net/>, accessed 03.2020).

To minimise the impact of a temporary structure on the given site at the university campus and guarantee an easy assembly and disassembly, lightweight aluminium rods and cables were chosen as the primary material. Each hypar module in the pavilion was discretised as ten rulings in both directions, other than ten parabolas curving upward and ten curving downward. As a result, the continuous surface of the pavilion turned into a gridshell. A pre-dimensioning of the structure under self-weight was initially carried out following the approach described in Section 3.1 and Section 3.2, using an equilibrium-based model and vector-based 3D graphic statics [18].

Several variations of the dimensions of the structural elements were tested; at each iteration, the current weight of the structure was calculated and applied to the structural model to update the load case. At the end of this iterative procedure, the rulings were set to aluminium rods with hollow section ($\Phi 8.0$ mm and 1.0 mm wall thickness), and the parabolic cables to stainless steel cables ($\Phi 2.0$ mm). The total mass of the structure accounted for 83.60 kg (Tables 1 and 2).

In order to check the elastic behaviour of the structure, a Finite Element Analysis (FEA) was then carried out using the software *Karamba3D* (<https://www.karamba3d.com/>, accessed 03.2020) (Fig. 10). The load cases considered in the analysis were the self-weight, a

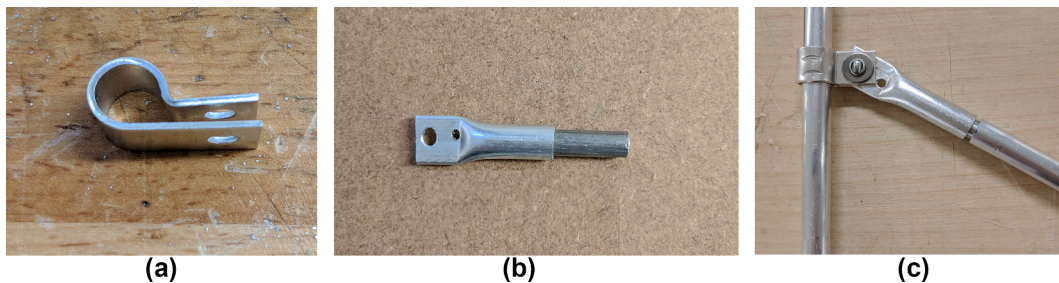


Fig. 12. The R-shape connection (left) and the rotating head are joined with (right) a rivet (below).

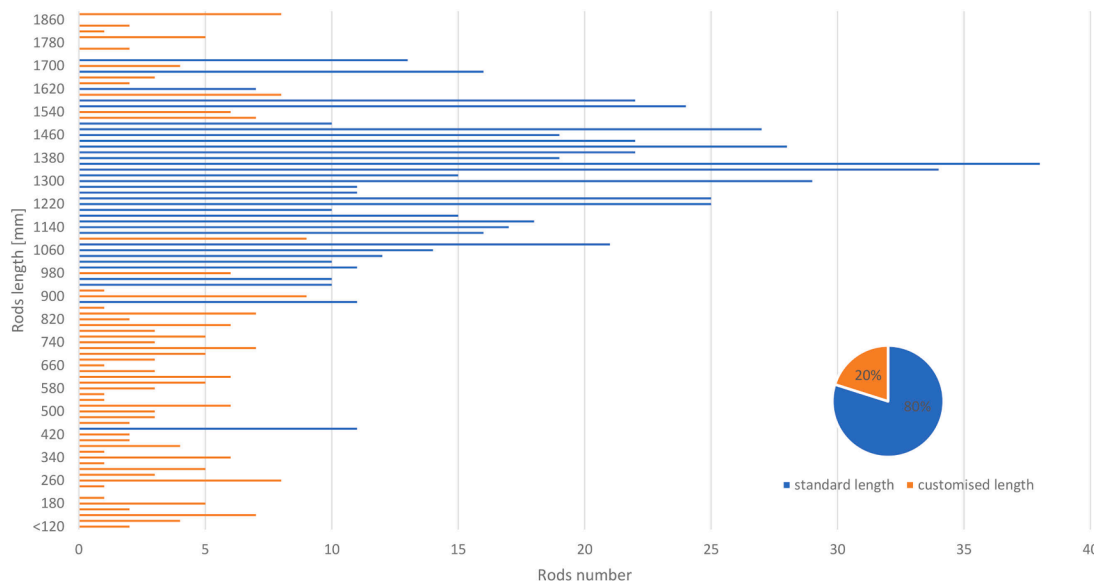


Fig. 13. Standard length and customised length of aluminium rods.

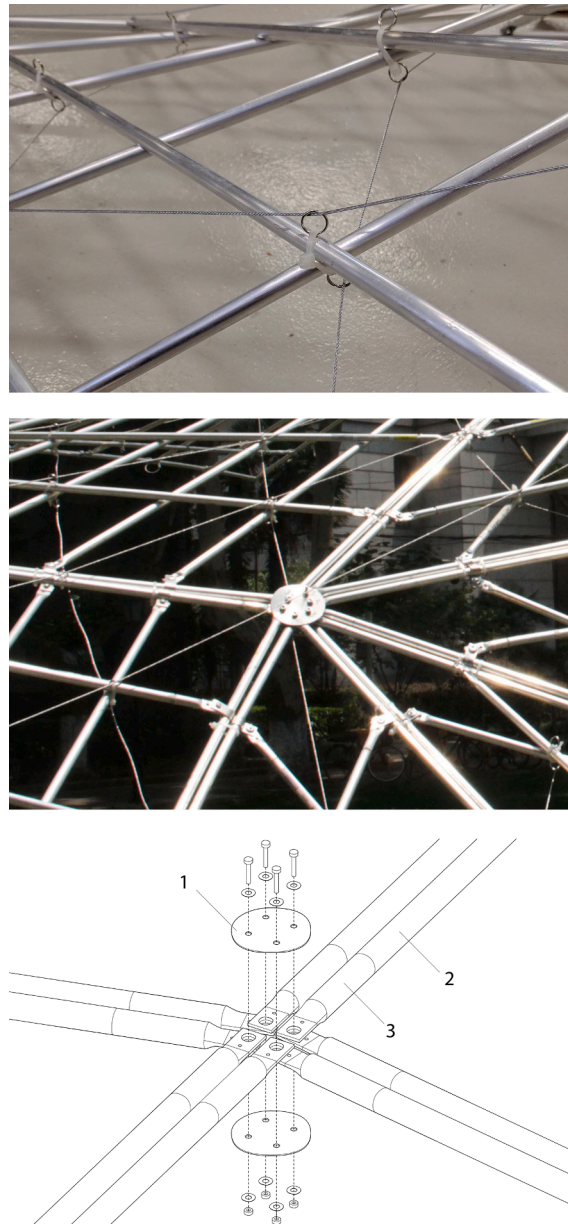


Fig. 14. Prestressing cables held by steel rings (top). Round plates to join several hypar modules at the nodes (middle). Assembly diagram of four hypars at a node (below): [1] round plate, [2] aluminium rod, [3] rotating head.

prestressing force applied to the steel cables as an initial strain of 0.3 mm/1.0 m, and a live load consisting of five point loads of 0.2kN each applied on the main vault of the gridshell, to simulate a mass hanging from the structure. In this loading condition, the pavilion showed a maximum displacement of 8.5 mm, a maximum tensile stress in the steel cables of 146 MPa, and maximum compression stress in the aluminium rods of -126 MPa.

4.2. Detailed design

At the level of detailed design, two types of joints were developed: joints connecting rulings and edges in each individual hypar, and joints connecting adjacent hypars. To simplify the fabrication of the joints and to allow using low-tech manufacturing approaches, customised joints have been avoided as much as possible.

In a generic hypar, the rulings always intersect the edges at various dihedral angles. To accommodate for this requirement, a standard joint with three hinges was designed, which could be easily adapted to

different angles between connected rulings and edges (Fig. 11). The standard joint consisted of two parts: the R-shape (Fig. 12) connector acting as a clamp, which was folded out of a 1-mm-thick aluminium strip; the rotating head (Fig. 12), which included two hinges and one telescopic connection (Fig. 11). The rotating head was flattened and punched on one side of a short Φ 8 mm aluminium rod (Fig. 12). It was joined to an R-shape connector with a rivet, which defined the first axis of rotation (Figs. 11, 12). To allow for manufacturing tolerances and another degree of rotation freedom, a short Φ 6 mm rod was inserted into an Φ 8 mm pipe (Figs. 11, 12). In this case, the head could rotate around and move along the axis of the ruling rod. The manufacturing of R-shape connectors and rotating heads took advantage of the relative softness and ductility of the aluminium in use.

In this way, all joints in a single hypar were standardised and the only variable to be considered during the fabrication process was the length of aluminium rods. In general, more than 800 pieces of aluminium rods were used in the construction of the Hypar Pavilion. To speed up the production of the rods, up to 80 percent of rods were cut



Fig. 15. Fabrication of one hypar with two wooden diagonals to keep four edges in the right position (above). Assembly of the pavilion (below) at the Southeast University of Nanjing (China).

into standard lengths (Fig. 13), with a difference less than 2 cm from one to another. The tolerance between the real length of a rod and the relative standard length could be taken into account by pulling out the rotating head through the telescopic connection. The other 20 percent of the rods (Fig. 13), whose lengths differed significantly from others, were cut according to their exact lengths. Moreover, standard rings were fixed with plastic ties to hold the prestressing cables (Fig. 14 top).

The joints between adjacent hypars were also standardised. The edges meeting at one node were simply connected with two round connection plates (Fig. 14 middle, below) – thanks to the coplanarity principle (Section 2.2), the edges of adjacent hypars were always located on the same plane. The radius of each round plate was constant and, therefore, the only variable was the location of the holes on the plates.

The use of simple mechanical joints in the Hypar Pavilion made it possible to assemble and disassemble the structure and possibly reuse all the rods and most of the joints for multiple service lives.

4.3. Construction of the hypar Pavilion

The construction of the Hypar Pavilion involved a team of sixteen students. All joints and rods were manufactured with simple hand tools, and the entire process from the prefabrication to the assembly took around forty hours.

Fabrication of the individual hypars Following a predefined assembly logic, the four edges were first connected with screws and then held in place in the exact position in space with two wooden diagonals



Fig. 16. Pictures of the assembled Hypar Pavilion at the Southeast University of Nanjing (China).



Fig. 17. The Hypar Pavilion was reassembled for a second exhibition in Dezhou, China.

(Fig. 15). The rulings were subsequently fixed at the edges with R-shape connections and screws, and the steel cables were inserted in the rings at the intersection points of every two rulings. After the production of each hypar was completed, the wooden diagonals were removed. However, the steel cables were not prestressed in this step, in order to count on certain flexibility of each hypar and allow for the required tolerance in the final assembly of the structure.

Assembly of the pavilion As described in Section 4.1, the whole pavilion was divided into two self-supported clusters, which were assembled separately and eventually joined together (Fig. 15). Hence, the hypars were assembled starting from the ground up to the top of the structure, taking advantage of the local stiffness of the double-curved geometry. The structure was restrained to the ground with multiple U-shaped steel pins. Throughout the whole assembly process, no scaffolding was required, except for some ladders to place the hypar modules located in the higher part of the structure (Fig. 15). After the entire structure was erected, the cables could be finally prestressed to complete the construction process. In this phase, the lengths of the cables were adjusted to match those calculated in the FEA model. Due to small fabrication and assembly imprecisions, the prestressing of the cables on site required some trial and error manual adjustments, until all the cables could be effectively tensioned.

Final outcome The Hypar Pavilion was exhibited for one month at the campus of the Southeast University of Nanjing (Fig. 16) and then disassembled and moved to another exhibition location. The disassembly process took place in around two hours by four people. After releasing all the prestressing cables and the round plates at the nodes, the 40 hypar modules could be stacked on top of each other and transported with a small truck to the city of Dezhou (China). The Hypar Pavilion was then reassembled for a second exhibition (Fig. 17). In this case, the pavilion was simply placed on top of a hard floor and stabilised using bracing cables since it was not possible to fix it to the ground rigidly.

The possibility to disassemble and reassemble the pavilion proved the success of the proposed temporary and reusable fabrication concept. In fact, this solution is in line with contemporary approaches to circular economy and builds upon a design paradigm based on an optimal use of materials, energy and resources [8]. In addition, it opens a discussion regarding concepts such as prefabrication versus in situ construction as well as customisation versus standardisation of building components. In this regard, while in most of the cases, customisation processes lead to the design and fabrication of complex and unique components, and standardisation processes relate to modular, repetitive and generic forms, the Hypar pavilion advocates for a hybrid paradigm. That is, the combination of standardised components with appropriate geometric and structural principles, generate customised and expressive forms that are, at the same time, easy to build, produce, assemble and disassemble. In this regard, the Hypar Pavilion introduced design strategies aiming at the conscious reuse of building materials.



Fig. 18. A smooth poly-hypar surface made with ferrocement. Six hypar modules were welded from steel rebars, assembled into the skeleton of a cantilevering shell (above), wrapped by a steel mesh (middle), and then covered with concrete (bottom).

5. Conclusion and future work

This article highlighted the design potentials of smooth poly-hypar surfaces when applied to the design of prestressed gridshells. As a double-curved and ruled surface, the special geometrical properties of the hypar guarantee structural integrity and stiffness to prestressed

gridshells designed as smooth poly-hypar surfaces. Structurally, a smooth poly-hypar gridshell behaves as a hybrid system between a prestressed cable network and a strut network. The prestressed cable network provides the rigidity to the surface, and the strut network, where all struts meeting at a node are always coplanar, can transmit internal forces to the supports without generating bending moments. Moreover, the ruled hypar modules in a smooth poly-hypar surface allow the implementation of low-tech construction techniques, as effectively demonstrated by the case study of the Hypar Pavilion.

The form and the structure of a smooth poly-hypar surface can be adapted to different material systems. In fact, an alternative manufacturing approach using the ferrocement technique introduced by the Italian engineer Pier Luigi Nervi [33] is currently under investigation for a second application of smooth poly-hypar surfaces (Fig. 18). The structural behaviour of a smooth poly-hypar surface as a continuous ferrocement shell is different from the prestressed gridshell case described in this article. In the ferrocement shell, the concrete part can generate compressive struts in the form of parabolas, while the steel rebars can resist tension. Benefiting from the ruled geometry, the fabrication of a smooth poly-hypar surface with ferrocement is relatively easy. Like a prestressed gridshell, it can be prefabricated in modules using straight element (rebars) and later assembled to form a larger surface structure. Before the concrete is poured, the reinforcing bars are wrapped with steel meshes, which act as lost formwork.

Declaration of Competing Interest

The authors declare that they have no known competing financial interests or personal relationships that could have appeared to influence the work reported in this paper.

Acknowledgements

The authors would also like to thank PhD student Zhang Junjun, and all the bachelor's and master's students that took part in the workshop at the Southeast University in Nanjing (China) in 2018 for their support and contribution to the manufacturing and assembly of the Hypar Pavilion. The executed research program is supported by China Scholarship Council (ID 201206090027). The fabrication of hypar pavillion is financed by National Natural Science Foundation of China (project ID 517778119).

References

- [1] Adriaenssens S, Brown N, Lowinger R, Hernandez J. Structural analysis of reinforced concrete folded hyperbolic paraboloid: a case study of the modern Miami marine stadium. *Int J Archit Heritage* 2012;8(4):498–516.
- [2] Aimond F. Thin shell roofs in the form of a hyperbolic paraboloid. *Le Génie Civil. (Le Génie Civil)* 1933;52(8).
- [3] Apeland K. 1962. "On the Analysis the Bending Stress in Shallow Hyperbolic Paraboloidal Shells." In *Proceeding of World Conference on Shell Structures*. San Francisco: World Conference on Shell Structures.
- [4] Bechthold M. Innovative surface structures: technology and applications. Abingdon: Taylor & Francis; 2008.
- [5] Beckh M. Hyperbolic structures: Shukhov's lattice towers - forerunners of modern lightweight construction. Chichester, West Sussex, United Kingdom: John Wiley & Sons Inc; 2015.
- [6] Bergdoll B, Pourtois C, Chiorino C, Olmo C, Nervi PL. Pier Luigi Nervi: architecture as challenge. Milan: Silvana Editoriale; 2010.
- [7] Billington DP. Thin shell concrete structures. New York: McGRAW-HILL Book; 1965.
- [8] Brütting J, Fivet C. Nothing is lost, nothing is created, everything is reused: structural design for a circular economy. *Struct Eng* 2020;98(1):74–81.
- [9] Candela F. General formulas for membrane stress in hyperbolic paraboloidal shells. *J Am Concr Inst* 1957;57(16):353–62.
- [10] Candela F. Structural application of hyperbolic paraboloidal shell. *J Am Concr Inst* 1951;51(20):397–415.
- [11] Cao T. Smooth Poly-Hypar Surface Structures. PhD Thesis. Zurich: ETH Zurich; 2019.
- [12] Cao, Ting, and Joseph Schwartz. 2014. "Prototypical Hypar: An Operative Form-making Method Based on Hyperbolic Paraboloids." In *Proceedings of the International Association for Shell and Spatial Structures (IASS)*. Amsterdam: IASS Conference 2014.
- [13] Cao, Ting, and Joseph Schwartz. 2017. "The Global Equilibrium of Hypar-combined Shells Based on the Method of Graphic Statics." In *Proceedings of the IASS Annual Symposium 2017*. Hamburg: IASS Conference 2017.
- [14] Chilton J. *The Engineer's contribution to contemporary architecture*, Heinz Isler. London: Thomas Telford; 2000.
- [15] Cremona L. *Polygon of forces and funicular polygon as reciprocal figures in graphic statics*. Oxford: Oxford University Press; 1890.
- [16] Culmann K. *Die graphische Statik*. Meyer und Zeller; 1866.
- [17] D'Acunto, Pierluigi, Patrick Ole Ohlbrock, Jean-Philippe Jasienski, and Corentin Fivet. 2016. "Vector-Based 3D Graphic Statics (Part I): Evaluation of Global Equilibrium." Tokyo: IASS Conference 2016.
- [18] D'Acunto, Pierluigi, Jean-Philippe Jasienski, Patrick Ole Ohlbrock, Corentin Fivet, Joseph Schwartz, and Denis Zastavni. 2019. "Vector-based 3D graphic statics: A framework for the design of spatial structures based on the relation between form and forces." *International Journal of Solids and Structures* 167: 58-70.
- [19] Domingo, Alberto, Carlos Lázaro, and P. Serna. 1999. "Design of a thin shell steel fiber reinforced concrete hypar roof." Madrid: IASS Symposium 1999.
- [20] Duarte Angel. *Angel Duarte, Junta de Extremadura, Consejería de Educación y Cultura*. Barcelona: Ediciones L; 1992.
- [21] Edward Allen, Waclaw Zalewski. *Form and forces: designing efficient, expressive structures*. Hoboken: Wiley; 2010.
- [22] Flöry, Simon, Yukie Nagai, Florin Isvoranu, Helmut Pottmann, and Johannes Wallner. 2012. "Ruled Free Forms." London: *Advances in Architectural Geometry 2012*, Springer.
- [23] Garlock, Maria E. Moreyra, and David P. Billington. 2008. Félix Candela : Engineer, Builder, Structural Artist. Princeton: Princeton University Art Museum.
- [24] Huhnen-Venedey Emanuel, Thilo Rorig. *Discretisation of asymptotic line parametrizations using hyperboloid surface patches*. *Geom Dedicata (Springer)* 2014;168(1):265–89.
- [25] Huhnen-Venedey, Emanuel, and Wolfgang K. Schief. 2013. "On Weingarten Transformations of Hyperbolic Nets." *International Mathematics Research Notices* 2015 (8).
- [26] Käferböck Florian, Pottmann Helmut. *Smooth Surfaces from Bilinear Patches: Discrete Affine Minimal Surfaces*. *Comput Aided Geom Des (Elsevier BV)* 2013; 2013(30):476–89.
- [27] Konstantatou, Marina, Pierluigi D'Acunto, and Allan McRobie. 2018. "Polarities in Structural Analysis and Design: N-dimensional Graphic Statics and Structural Transformations." *International Journal of Solids and Structures (Proceedings of the IASS Annual Symposium 2017)* 2018 (152-153): 272-293.
- [28] Maxwell JC. *On reciprocal figures, frames and diagrams of forces*. *Phil Mag* 1864; 250(61):27.
- [29] Mendoza, Marisela Ramos. 2011. "Félix Candela's legacy: an investigation of Félix Candela's work and its legacy to the sociocultural heritage and public identity of the contemporary society in Mexico and the UK." In *RIBA Education Yearbook 2011*, edited by J.-P. NUNES, 126-131. London: Royal Institute of British Architects.
- [30] Mortenson Michael E. *Geometric modeling*. New York: Industrial Press; 2006.
- [31] Mueller G. *Nonlinear analysis of reinforced concrete hyperbolic paraboloid shells*. Berkeley: Department of Civil Engineering, University of California; 1977.
- [32] Muttoni A, Schwartz J, Thürlimann B. *Design of concrete structures with stress fields*. Basel: Birkhäuser; 1997.
- [33] Nervi Pier Luigi. *Pier Luigi Nervi: aesthetics and technology in building*. Cambridge: Harvard Press; 1966.
- [34] Parme Alfred L. *Hyperbolic paraboloids and other shells of double curvature*. *Struct Div (Am Soc Civ Eng)* 1956;82(5):1–32.
- [35] Ramaswamy GS. *Design and construction of concrete shell roofs*. New York: McGraw-Hill; 1968.
- [36] Schnobrich WC. "Analysis of Hyperbolic Paraboloid Shells." *Concrete Thin Shells (American Concrete Institute) ACI Special Publication (P-28)*; 1971: 275-312.
- [37] Schnobrich WC. "Bending Theory." In *Hyperbolic Paraboloid Shells: State of the Art*, by Jack Christiansen, edited by Jack Christiansen, 5. Michigan: American Concrete Institute; 1988b.
- [38] Schnobrich WC. *Hyperbolic Paraboloid Shell Structures*. In: Christiansen Jack, editor. *Hyperbolic Paraboloid Shells: State of the Art*, by Jack Christiansen. Detroit: American Concrete Institute; 1988. p. 1–15.
- [39] Scordelis AC, Ramirez HD, Ngo D. Membrane stresses in hyperbolic paraboloid shells having a parallelogram shape in plan. *ACI Journal (American Concrete Institute)* 1969;66(87):994–1000.
- [40] Scordelis AC, Ramirez HD, Ngo D. Membrane stresses in hyperbolic paraboloid shells having an arbitrary quadrilateral shape in plan. *ACI J (Am Concr Inst)* 1970; 67(4):994–1000.
- [41] Wallner Johannes. *Discrete Asymptotic Nets and W-congruences in Plücker Line Geometry*. *J Geom Phys (Elsevier)* 2001;39(1):9–29.